TIRF Microscopy as a Screening Method for Non-Specific Binding on Surfaces

Christy Charlton[1*], Vladimir Gubala[1], Ram Prasad Gandhiraman[1], Julie Wiechecki[1], Nam Cao Hoai Le[1], Conor Coyle[1,2], Stephen Daniels[1,2], Brian D. MacCraith[1], David E. Williams[1,3]

[1] Biomedical Diagnostics Institute, Dublin City University, Dublin 9, Ireland
[2] National Centre for Plasma Science and Technology, Dublin City University, Dublin 9, Ireland
[3] MacDiarmid Institute for Advanced Materials and Nanotechnology, Department of Chemistry, University of Auckland, Private Bag 92019, Auckland 1142, New Zealand

* Corresponding author:
Biomedical Diagnostics Institute, Dublin City University
National Center for Sensor Research, Research and Engineering Building
Glasnevin, Dublin 9, Ireland;
email address: christy.charlton@dcu.ie;
tel: +353-1-700-6352;
fax: +353-1-700-6558

Abstract
We report a method for studying nanoparticle-biosensor surface interactions based on Total Internal Reflection Fluorescence (TIRF) Microscopy. We demonstrate that this simple technique allows for high throughput screening of non-specific adsorption (NSA) of nanoparticles on surfaces of different chemical composition. Binding events between fluorescent nanoparticles and functionalized Zeonor® surfaces are observed in real-time, giving a measure of the attractive or repulsive properties of the surface and the kinetics of the interaction. Three types of coatings have been studied: one containing a polymerized aminosilane network with terminal $–NH_2$ groups, a second film with a high density of –COOH surface groups and the third with sterically restraining branched poly(ethylene)glycol (PEG) functionality. TIRF microscopy revealed that the NSA of nanoparticles with negative surface charge on such modified coatings decreased in the following order $–NH_2$ > -branched PEG > -COOH. The surface specificity of the technique also allows discrimination of the degree of NSA of the same surface at different pH.

Keywords
Total Internal Reflection, Fluorescence, Microscopy, Non-Specific Binding, Surface-Particle Interaction

1. Introduction

Current research in biomedical diagnostics is directed at inexpensive, highly sensitive, miniaturized devices, in which usually disposable substrates or chips are used. Such devices are required to measure analytes in microliter volume samples, typically at picomolar level. In fluorescence-based assays, the signal can be greatly enhanced with

the use of dye doped nanoparticles as fluorescent labels [1-4]. However, in a successful diagnostics device, signal-to-noise ratio is paramount to its performance and effectively controls the sensitivity. Controlling the noise and background contribution, dictated by non-specific binding of the non-analyte constituents of the sample remains very challenging. The chemical composition of the substrate surface and its interactions with the active surface area of the dye-doped nanoparticles, therefore, play a key role in the performance of diagnostic platform. In this work, we focus on surface functionalization of the substrate Zeonor®, a cyclo-olefin polymer (COP), which is characterized by ease of injection molding for biochip fabrication and relatively low autofluorescence, which is an important factor for fluorescence-based applications including TIRF microscopy.

Total Internal Reflection Fluorescence (TIRF) microscopy [5] is presented here as a very useful and fast method to compare non-specific adsorption of detection molecules on different surfaces. This method allowed for rapid screening of surfaces to find their ability to prevent non-specific binding. Total internal reflection occurs an any interface between materials of different refractive index inside the material of higher refractive index provided the angle of incidence of the light is above the critical angle defined as:

$$\theta_c = \arcsin(\frac{n_2}{n_1}) \qquad (1)$$

where n_1 is the refractive index of the high refractive index material (Zeonor® ≈ 1.5 in our case but this could also be glass or other polymers) and n_2 is the refractive index of the low index material (typically water = 1.3 or air = 1). Upon total internal reflection, an evanescent field is established which penetrates a small distance (in our case, approx. 100 nm) into the low refractive index material. TIRF is typically achieved by coupling excitation light to the surface through either a prism or the microscope objective [5]. More recently, excitation light has been coupled into a waveguide and microscopic measurements have been performed on the waveguide surface [6]. In our experiments, light is coupled directly into a 2.5 x 7 x 0.2 cm slide fabricated from cyclo-olefin polymer, known commercially as Zeonor®, to allow for characterization of surface coatings by simply counting the adsorbed particles on the substrate. TIRF allows surface-particle interactions to be investigated, as it excites only particles within the evanescent field of the excitation light, providing surface specificity and improving signal to noise compared with conventional microscopy [5]. In this work, we use TIRF in a novel way to screen surfaces for the levels of non-specific binding in a particular system.

We have recently reported that fluorescent nanoparticles are very useful as labels in immunoassays to achieve improvements both in assay kinetics and sensitivity [7-9]. However, these particles typically have a negatively charged surface due to surfactants used to stabilize them and avoid aggregation [10,11]. This can cause particles to bind non-specifically due to charge attraction to surfaces commonly used for protein absorption such as 3-aminopropyltriethoxy silane (APTES) [12-14]. As illustrated on Scheme 1, APTES coated substrates contain a high density of amine groups that are in equilibrium between the charged $–NH_3^+$ and neutral $–NH_2$ form. Whether this equilibrium is shifted towards its charged or neutral species depends on the pH of the environment. At physiological pH, it is the effect of the positively charged $–NH_3^+$ groups that governs the surface characteristics. It is therefore expected that the physical adsorption of negatively charged nanoparticles on such a surface would be high due to a favourable electrostatic attraction with the $–NH_3^+$ groups. On the other hand, a film that is

intrinsically negatively charged, such as one with –COOH functional groups, is expected to significantly reduce the non-specific adsorption of the nanoparticles. Indeed, the carboxy group is mostly deprotonated (shown as $–COO^-$ in Scheme 1) at pH ~ 7. Such coating was prepared by co-polymerization of acrylic acid and tetraorthosilicate (TEOS) using a method called plasma enhanced chemical vapour deposition (PECVD). In this process, TEOS was grafted onto a Zeonor substrate and allowed to cross-link with molecules of acrylic acid. The polymerization reaction was initiated by plasma and resulted in the formation of exceptionally stable, hydrophilic film with high density of –COOH groups.

Polyethylene(glycol) derivatives are also known in surface chemistry as effective suppressors of non-specific binding of biomolecules [15-18]. Their function is associated less with electrostatic forces but rather with vast hydration and effects of change of configurational entropy when large molecules adsorb upon them. We have modified an APTES film with a branched and sterically demanding PEG derivative (Scheme 1) and compared the physisorption of nanoparticles with both charged coatings. Surface particle density and binding rate constants were used as a measure of surface-particle attraction; the effect of the pH was also investigated. We show that kinetic data can be extracted from the real-time binding curves of the particles on each surface. This tool could be used to investigate surface binding kinetics, which are another key parameter in diagnostic devices [19,20].

2. Materials and Methods

2.1 Fluorescent Particles

Carboxyl functionalized yellow fluorescent nanoparticles (110 nm diameter, 1.0 % w/v solution in water, emission max at 490 nm) were purchased from Kisker Biotech (Steinfurt, Germany). The stock solution was diluted to a final concentration of 1×10^{-4} mg/mL in deionized water for the surface comparison measurement and in 0.1 M 2-(N-morpholino)ethanesulfonic acid (MES) buffer at pH values of 3 and 7 for the pH comparison measurements. Buffers were made using 0.1 M MES and adjusted with HCl to pH 3 and with NaOH to pH 7.

2.2 NP – anti-hCG conjugation

1mg of fluorescent amine functionalized (170 nm diameter) fluorescent polystyrene NPs was washed two times in water by centrifugation (17,000 rpm, 10 min), then resuspended in 0.5 mL of 0.1 M $NaHCO_3$ buffer at pH=8.5. To this mixture, 117 μg of monocolonal anti β-hCG antibody was added and allowed to physically adsorb on the surface of the polystyrene NPs in the course of 3 hours. The unreacted, free anti β-hCG in solution was removed by centrifugation and the mixture was washed three times with phosphate buffered saline at pH=7.4. For longer term storage, bovine serum albumine (BSA) would be added to the sample and it would be kept in a dark, cold place.

2.3 Surface Preparation

Microscope size slides (2.5 x 7.0 x 0.2 cm) were made of Zeonor® and supplied by Åmic and Sigolis (Uppsala, Sweden). One set of slides were coated with a 93 Å thick layer of polymerized molecules of 3-aminopropyltriethoxy silane (APTES) and ethylenediamine

(EDA) by Plasma Enhanced Chemical Vapour Deposition (PECVD) [21]. PEG functionalized slides were prepared by immersing the APTES coated slides in a 1 mM solution of TMS(PEG)$_{12}$ with 2.5 + 5.2 nm long spacer arm, purchased from Pierce Chemicals. COOH functionalized Zeonor® slides were prepared using PECVD [22] technique by co-polymerization of tetraorthosilicate and acrylic acid. A cartoon of surfaces coatings are shown in Scheme 1. Our PECVD coated surfaces have been shown to have a roughness of approx. 1 nm [12,13]. This roughness is minimal and does not effect the surface measurements presented in this work.

2.4 TIRF setup

A 473 nm blue laser with 50 mW maximum output (Photop Technologies Inc, Fujian, China) was coupled to the Zeonor® microscopy slide via a BK7 prism (BRP-5, Newport, Oxfordshire, UK) index matched to the slide with immersion oil. Light entered the slide at an angle of 15° from horizontal giving an angle of reflection at the Zeonor®/water interface of approximately 65° from the vertical, which is above the critical angle of 61° needed for total internal reflection. This setup was placed above the objective on an Olympus IX81 (Olympus, Essex, UK) inverted fluorescence microscope. A drop of fluorescent particle solution was placed on the top slide surface at a location where the laser beam was being reflected from the surface giving an evanescent field at that point. When the particles reach the surface, they are excited by the evanescent field and emit fluorescence which is collected through the slide from below. The TIRF setup is shown schematically in Figure 1a and pictorially in Figure 1b.

2.5 Imaging and Particle Counting

A 20x 0.50 NA objective (UPlanFLN, Olympus, Essex, UK) was used giving a viewing area of 0.144 mm^2. An Olympus U-MWIBA filter was used to block excitation light of the laser and image the fluorescence emitted by the particles. Images were recorded every 10 seconds for 2000 seconds with a 5 second exposure time on an Olympus DP71 camera. Image color was adjusted using ImageJ software to remove background noise before particles were counted using Matlab image processing software.

3. Results and discussion

The fluorescent nanoparticles used in our experiments have carboxyl functional groups that are mostly negatively charged in water or buffered solutions at pH ~ 7 for improved colloidal stability (zeta potential was measured to be -36 mV for particles in pH 7 MES buffer). Three types of coatings were studied. Two sets with deposited molecules that can be either positively (protonated -NH_2 groups) or negatively (deprotonated -COOH groups) charged under the measured conditions. A third coating had neutral PEG grafted on top of the APTES film forming a relatively thick (7.7 nm), sterically demanding blocking layer with the ability to interact with large number of water molecules. Plain Zeonor® is a relatively hydrophobic material with a water contact angle > 90 degrees. Treatment of Zeonor® with the chemicals to obtain coatings as described above rendered the surface more hydrophilic with water contact angles decreasing in the order –NH_2 > PEG > -COOH (Table 1).

Figure 2 shows three selected images illustrating the accumulation of NPs on the studied surfaces over time. Note that the recorded image of a particle is a convolution of the geometric particle image of diameter M_{dp}, with the diameter of the diffraction-limited point spread function (PSF) of the recording optics, $d_{s\infty}$. The diameter of the diffraction-limited PSF of an infinity-corrected system can be calculated as [23]:

$$d_{s\infty} = 1.22M\lambda\left[\left(\frac{n_o}{NA}\right)^2 - 1\right]^{1/2} \quad (2)$$

where n_0 is the refractive index of the immersion medium (air, $n_0 = 1$), $NA = 0.5$ and $M = 20$ are the numerical aperture and magnification of the objective lens, respectively, $d_p = 110$ nm is the particle nominal diameter and $\lambda = 490$ nm is the wavelength of emission maxima of the fluorescent particle. For the system reported here, the diffraction-limited PSF size is calculated to be 20.7 μm.

The particle image diameter can be obtained by approximating M_{dp} and $d_{s\infty}$ as Gaussians [24]:

$$d_e = \left[M^2 d_p^2 + d_{s\infty}^2\right]^{1/2} (3)$$

The particle image diameter is calculated to be 20.8 μm, which projected back to the surface of the substrates, would correspond to 1.04 μm. This explains the apparent size of the particles in Figure 2.

Image processing algorithms allowed a particle count to be determined for each image giving the number of particles on the surface at each individual time frame. The results were then plotted as a function of NP count vs. time for APTES, PEG, and COOH surfaces as shown in Figure 3a. As expected, the negatively charged NPs were mostly attracted to the amine terminated APTES surface groups. The average density of surface bound NPs at a time of 2000 sec was nearly 28 times higher than that of the negatively charged –COOH surface. If the particle coverage on the surface is sufficiently low that the particle accumulation on the surface is not affected by particle-particle interactions or by the approach to the jamming limit, then the accumulation can be described as a simple first-order chemical reaction. The rate constant can be obtained by fitting and determination of the initial rate of rise. The difference between the relative binding rate constant of the two charged surfaces was more than 40 fold (Table 1, Figure 4). In comparison with the APTES film, the neutral PEG modified slides showed only a 4 fold decrease in the number of adsorbed NPs and 3 fold decrease in the binding rate constant $(k_{2000})_{rel}$. Despite the positive effect of the PEG layer acting as a steric, highly hydrated barrier, we reason that it is the electrostatic interactions that dominate the physical adsorption of the negatively charged nanoparticles on the substrate surface.

With that in mind, we further investigated the effect of varying solution pH on the NP accumulation. Since the pKa value for the –COOH groups is in the range of 4.2 – 5.0, at pH values below this, the equilibrium between –COOH and $–COO^-$ will be shifted to the protonated form, hence reducing the charge effect of the film. As a consequence, more NPs were expected to accumulate on such surface. This phenomenon was demonstrated in buffered solution at pH = 3 and summarized on Figure 3b. By neutralizing the charge both on the surface of the particles and on the substrate, the average surface density of the bound NPs along with its binding rates increased by a factor of 4.

For the negatively charged, neutral or near-neutral surfaces, the imaging revealed that the surface was in small, isolated patches not compositionally uniform. We deduce this from the fact that some particles adhered very rapidly (within the time taken to focus the microscope - ~ 10s) after which the accumulation rate decreased significantly. This effect was particularly noticeable for the nominally neutral PEG-modified surface (figure 3a) and for the carboxylate-coated surface at pH7 (figure 3b).

In fluorescence-based immunoassays, the dye-doped nanoparticles are sensitized with the detection antibody, which obviously has an impact on the overall charge of the label. Therefore, we reviewed the effect of non-specific binding of antibody-sensitized NPs on the carboxyl functionalized surface. Monoclonal anti β-hCG antibody was immobilized on the surface of the fluorescent NPs and their accumulation on the –COOH surface (so far confirmed to be the most effective in reducing non-specific binding) was monitored in course of 1000 sec. The results are summarized on Figure 3c, comparing the effect of unmodified NPs with the antibody-sensitized NPs. As the isoelectric point of anti-hCG antibody is below the pH of the solution (7), it is assumed that its overall charge is negative. Consequently, the antibody immobilized on the NP surface did not drastically change the total negative charge of the particle. The net result is only a small increase in non-specific binding when compared to that of unmodified NPs, what is ultimately a very important parameter for improving signal-to-noise ratio in any diagnostics device.

5. Conclusion

We have shown that TIRF microscopy can be used as a simple rapid screening tool for non-specific interactions between fluorescent particles and surfaces. This method can be used to determine what surface characteristics are the most optimal for a given application, resulting in the lowest levels of non-specific binding. From our studied surfaces, it is the like-charge electrostatic repulsion between substrate and NPs that showed the strongest effect in decreasing the background signal. The charge-charge repulsions greatly outperformed the effect of PEG coatings that function on the basis of steric hindrance and water hydration. COOH functionalized surfaces were found to provide enough charge repulsion even to the antibody coated particles, leading to very low non-specific binding. The TIRF technique is clearly extremely useful for the study of the surface related interactions in a full immunoassay.

Acknowledgement

The authors wish to thank Martin Sommers for assistance with image processing. We are grateful to Science Foundation Ireland (Grant No. 05/CE3/B754) for funding.

Figure Captions

Scheme 1: Schematic of surface functionalizations: a) APTES, b) PEG and c) Carboxyl

Table 1: Water contact angle values of the prepared coatings, the average particle density for each surface calculated at a time of 2000 seconds and the corresponding binding rate constants.

Figure 1: a) Schematic of TIRF setup; b) Photos of TIRF setup

Figure 2: Images of particle accumulation on surface for an APTES coated slide (note: color brightened to enhance particle visibility)

Figure 3: Graph of particle count vs. time for carboxylated particles accumulating on each of the following surfaces: a) APTES (□), PEG (○) and COOH (▲); b) COOH at pH 3 (○) COOH at and pH 7 (●); c) COOH surface with COOH functionalized particles (△) COOH surface with hCG conjugated particles (●)

Figure 4: Relative binding rate constant of the studied surfaces.

Figures

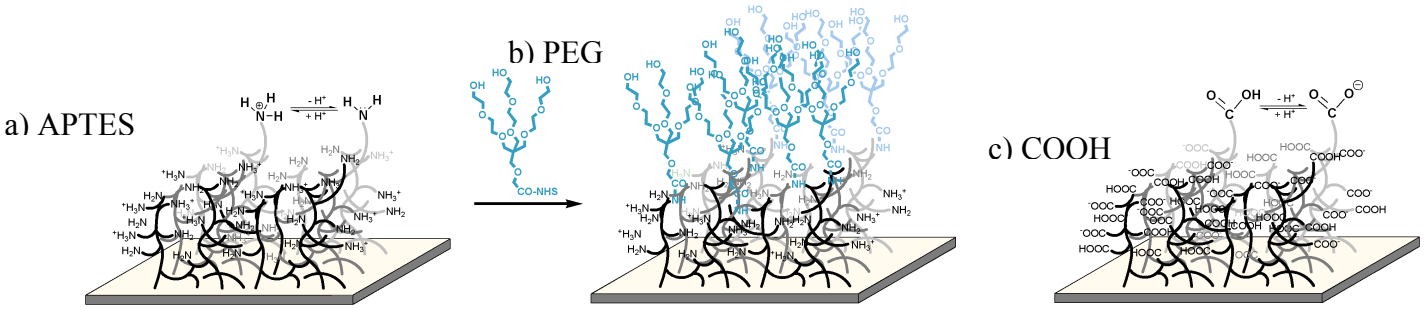

Scheme 1

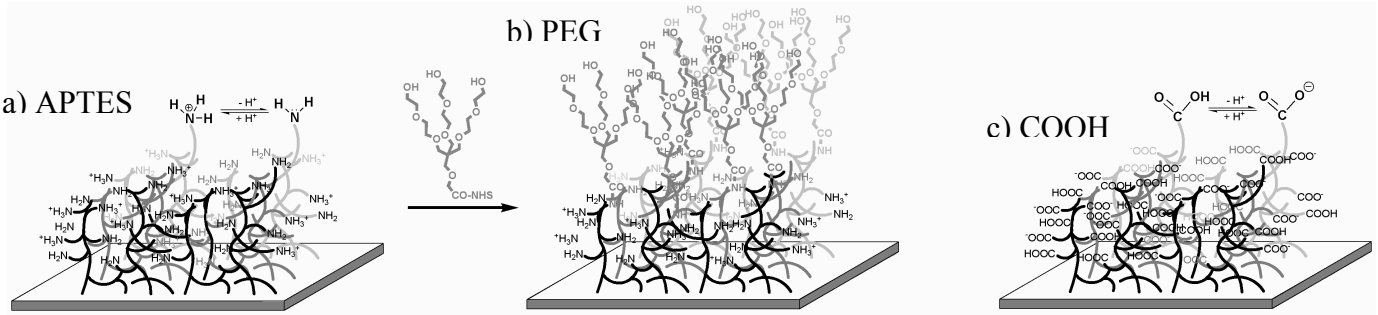

Scheme 1 black and white for print

Surface	Water contact angle (degrees)	Average Surface NP Density (particles / mm^2)	Binding rate constant k_{2000} (s^{-1})[b]
APTES	55.0 ± 2.6	5727 ± 185	83 x 10^{-2}
TMS(PEG)12	38.3 ± 1.5	1537 ± 387	25 x 10^{-2}
COOH at pH 7	9.9 ± 0.2	206 ± 16	2 x 10^{-2}
COOH at pH 3		951 ± 84	8 x 10^{-2}
COOH at pH 7[a]		387 ± 53	6 x 10^{-2}

[a] the nanoparticles in this experiment were sensitized with monoclonal anti-hCG antibody and the values were analyzed at a time of 1000 sec

[b] The binding rate constants were calculated by fitting a linear regression to the first 250 seconds of each measurement curve shown in Figure 3

Table 1

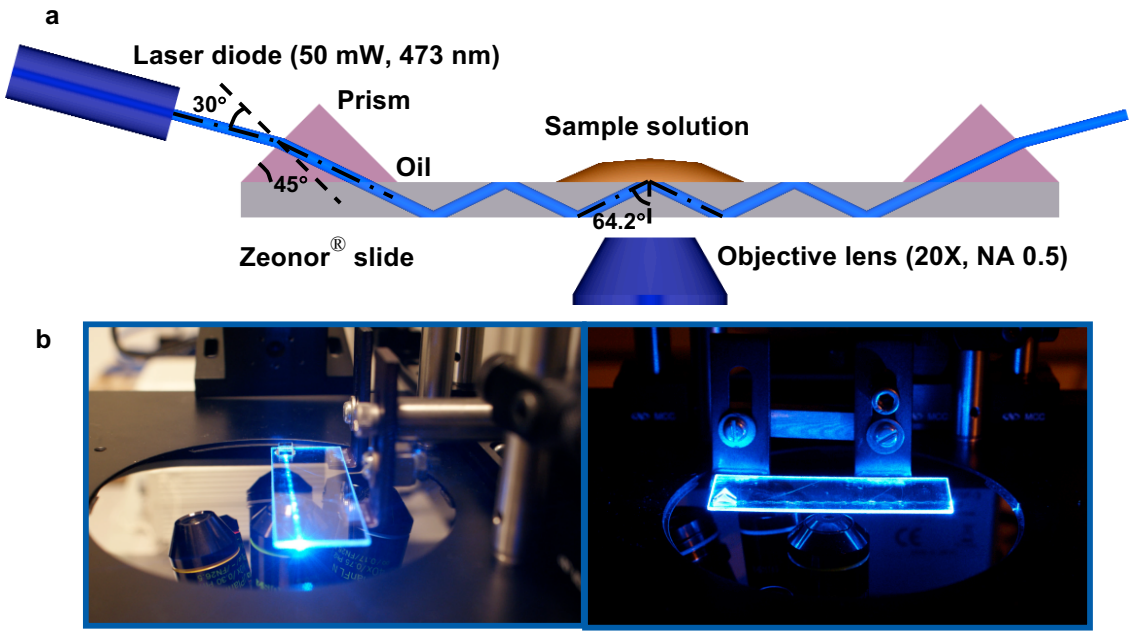

Figure 1

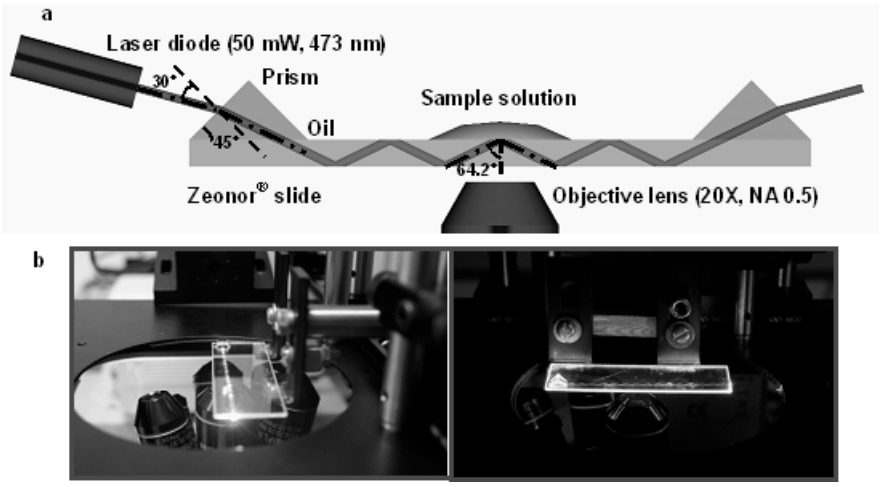

Figure 1 black and white for print

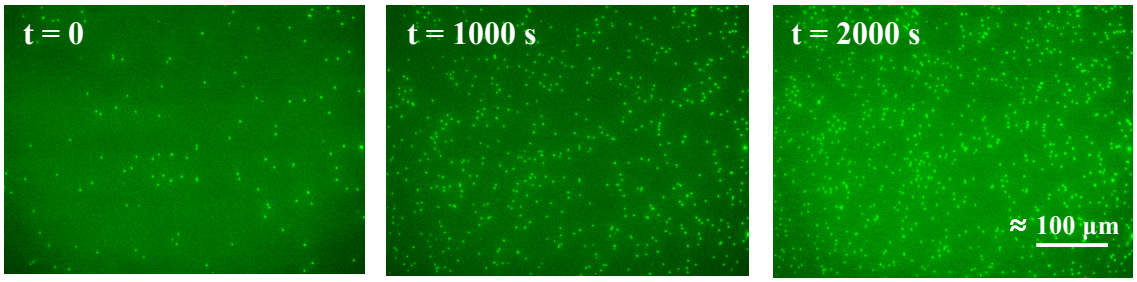

Figure 2

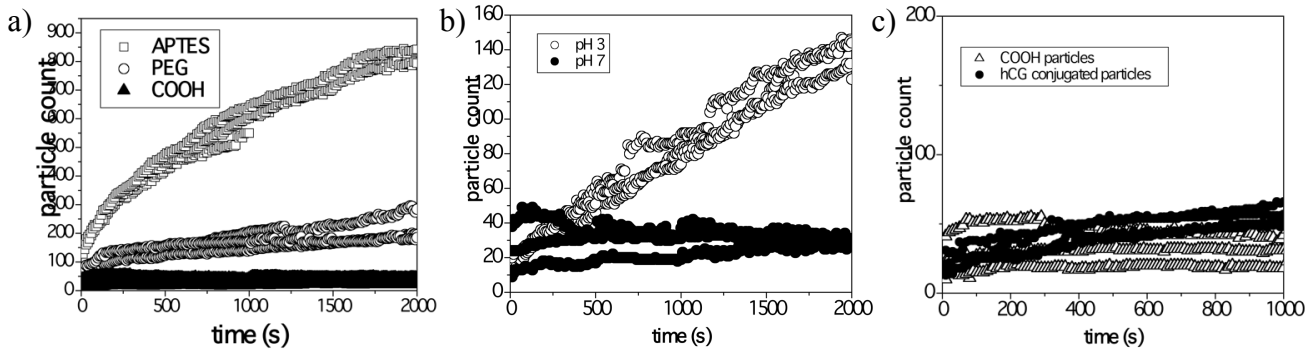
a)
APTES
PEG
COOH
particle count
time (s)
b)
pH 3
pH 7
particle count
time (s)
c)
COOH particles
hCG conjugated particles
particle count
time (s)

Figure 3

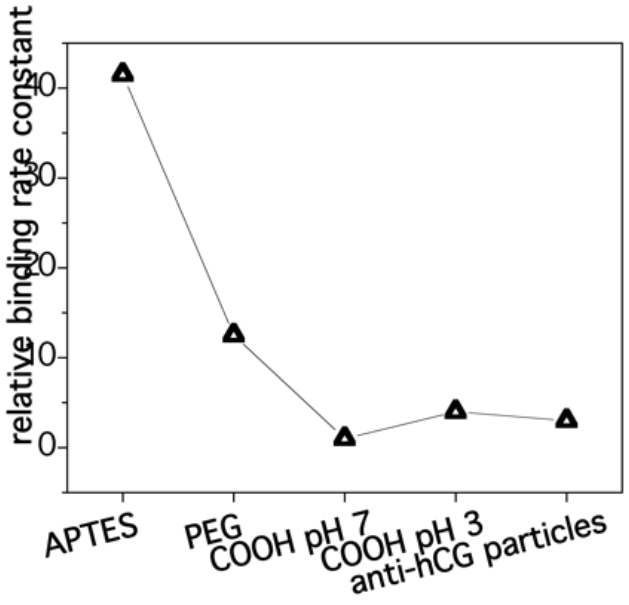
relative binding rate constant
40
30
20
10
0
APTES
PEG
COOH pH 7
COOH pH 3
anti-hCG particles

Figure 4

References

1. A. Burns, H. Ow, U. Wiesner, Chem. Soc. Rev. 35 (2006) 1028.
2. C. E. Fowler, B. Lebeau, S. Mann, Chem. Commun. (1998) 1825.
3. V. Gubala, X. Le Guevel, R. Nooney, D. E. Williams, B. D. MacCraith, Talanta 81 (2010) 1833.
4. J. L. Yan, M. C. Estevez, J. E. Smith, K. M. Wang, X. X. He, L. Wang, W. H. Tan, Nano Today 2 (2007) 44.
5. H. Schneckenburger, Current Opinion in Biotechnology 16 (2005) 13.
6. A. Hassanazadeh, M. Nitsche, S. Mittler, S. Armstrong, J. Dixon, U. Langbein, Applied Physics Letters 92 (2008) 233503.
7. C. Crean (née Lynam), V. Gubala, R. O'Kennedy, D. E. Williams, submitted to Colloids Surf., B. (2010)
8. V. Gubala, C. Lynam, R. Nooney, S. Hearty, B. McDonnell, R. O'Kennedy, D. E. Williams, submitted to Anal. Bioanal. Chem. (2010)
9. C. McDonagh, O. Stranik, R. Nooney, B. D. MacCraith, Nanomedicine 4, 6 (2009) 645.
10. R. J. Hunter, Foundations of Colloid Science, Vol. 1. Oxford University Press, New York, 1987
11. R. I. Nooney, C. M. N. McCahey, O. Stranik, X. Le Guevel, C. McDonagh, B. D. MacCraith, Anal.Bioanal. Chem. 393, 4 (2009) 1143.
12. R. P. Gandhiraman, C. Volcke, V. Gubala, C. Doyle, J. Raj, L. Basabe-Desmonts, M. Iacono, R. I. Nooney, G. Herzog, S. Daniels, D. W. M. Arrigan, B. James, D. E. Williams, J. Mater. Chem. 20 (2010) 4116
13. V. Gubala, R. P. Gandhiraman, C. Volcke, C. Doyle, C. Coyle, B. James, S. Daniels, D. E. Williams, Analyst 135 (2010) 1375
14. C. Jonsson, M. Aronsson, G. Rundstrom, C. Pettersson, I. Mendel-Hartvig, J. Bakker, E. Martinsson, B. Liedberg, B. MacCraith, O. Ohman, J. Melin, Lab Chip 8 (2008) 1191.
15. P. K. Ajikumar, J. K. Ng, Y. C. Tang, J. Y. Lee, G. Stephanopoulos, H-P. Too, Langmuir 23 (2007) 5670.
16. T. McPherson, A. Kidane, I. Szleifer, K. Park, Langmuir 14 (1998) 176.
17. S. Pasche, J. Voros, H. J. Griesser, N. D. Spencer, M. Textor, J. Phys. Chem. B 109, 37 (2005) 17545.
18. A. J. Pertsin, M. Grunze, Langmuir 16 (2000) 8829.
19. K. E. Sapsford, Z. Liron, Y. S. Shubin, F. S. Ligler, Analytical Chemistry 73, 22 (2001) 5518.
20. K. E. Sapsford, F. S. Ligler, Biosensors and Bioelectronics 19 (2004) 1045.
21. G. Ram Prasad, S. Daniels, D. C. Cameron, B. P. McNamara, E. Tully, R. O'Kennedy, Surface & Coatings Technology 200 (2004) 1031.
22. C. Coyle, et al., 2010 patent and manuscript in preparation.
23. C.D. Meinhart and S.T. Wereley, Measurement Science and Technology 14 (2003) 1047.
24. R. J. Adrian, Annual Review of Fluid Mechanics 23 (1991) 261.